Applied Catalysis B: Environmental 146 (2014) 227–236

Contents lists available at ScienceDirect

Applied Catalysis B: Environmental

journal homepage: www.elsevier.com/locate/apcatb

Partial oxidation of methane on Ni_xAlBEA and Ni_xSiBEA zeolite catalysts: Remarkable effect of preparation procedure and Ni content

Karolina A. Chalupka[a,b,c,*], Wojciech K. Jozwiak[a], Jacek Rynkowski[a], Waldemar Maniukiewicz[a], Sandra Casale[b,c], Stanislaw Dzwigaj[b,c,**]

[a] Lodz University of Technology, Institute of General and Ecological Chemistry, Zeromskiego 116, 90-924 Lodz, Poland
[b] UPMC Univ Paris 06, Laboratoire de Réactivité de Surface, Case 178, Site d'Ivry-Le Raphaël, 3 rue Galilée, 94200 Ivry sur Seine, France
[c] CNRS-UMR 7197, Laboratoire de Réactivité de Surface, Case 178, Site d'Ivry-Le Raphaël, 3 rue Galilée, 94200 Ivry sur Seine, France

ARTICLE INFO

Article history:
Received 30 October 2012
Received in revised form 23 April 2013
Accepted 7 May 2013
Available online 16 May 2013

Keywords:
POM reaction
Synthesis gas
Ni catalysts
BEA zeolite

ABSTRACT

This work reports on the investigation of the influence of the preparation procedure and Ni content on partial oxidation of methane to synthesis gas. For this purpose the Ni-containing zeolite catalysts were prepared by two different methods: a conventional wet impregnation method (Ni_xAlBEA series), in which Ni ions were introduced mainly in the extra framework position and a two-step postsynthesis method (Ni_xSiBEA series), which allowed incorporating Ni ions into the zeolite framework. Calcined Ni_xAlBEA and Ni_xSiBEA zeolite catalysts showed different physicochemical properties and thermal stability in POM reaction. The C-Ni_xSiBEA catalysts demonstrated very high activity (100% conversion of CH_4) and selectivity to CO (up to 100%) and resistance to deactivation. Moreover, they were much more stable than C-Ni_xAlBEA catalysts. On neither of 2 series of catalysts carbon deposition was observed in contrast to the catalysts usually used and described in literature. The TPR-H_2 experiments showed the presence of different Ni species in C-Ni_xSiBEA and C-Ni_xAlBEA catalysts and XRD analysis proved that dealumination and high temperature treatment did not destroy the zeolite structure.

1. Introduction

The production of hydrogen and synthesis gas has been widely studied in recent years because of their potential application as sources of clean energy [1–3].

The synthesis gas (syn-gas), being CO and H_2 mixture, is called a strategic substrate of the XXI century. It has an industrial application to fuel (Fischer–Tropsch synthesis) and chemical production [4]. Syn-gas is produced from natural gas, carbon, biomass and refinery waste in gasification and reforming processes. One of the most popular ways of syn-gas production is partial oxidation of methane (POM) [1–5]. This reaction makes it possible to obtain syn-gas with a molar ratio of $CO:H_2 = 1:2$, proper to Fischer–Tropsch or methanol synthesis. The advantages of POM reaction are high syn-gas yield and CO selectivity, which allow to avoid an expensive process of CO_2 and H_2O removal from syn-gas.

Ni, Pt, Ru and Rh supported Al_2O_3 and SiO_2 are well known as catalysts of POM reaction [2,6]. However, the deactivation of these catalysts by carbon deposition and sintering is still the serious problem. This process may be related to harsh conditions under which the reaction is carried out (a low O:C ratio and high temperature) [2]. The solution is to obtain Ni catalyst with a small size of particles and high specific surface area, which ensures a good dispersion of metal species as well as better resistance to sintering.

Aluminosilicate materials are widely used in heterogenous catalysis. These materials proved to be very good supports for preparation of metal containing catalysts due to their well defined crystalline structure, high surface area and a possibility to modify their acidity and catalytic activity [7–9]. Their high surface area, good dispersion of metals and superior coke resistance make metal-containing zeolite catalysts useful in various catalytic processes, particularly those related to environmental protection and renewable energy [10].

For these various reasons we have applied the zeolite catalysts in POM reaction although it was believed that zeolite materials are not good support for preparation the catalysts of POM or methane reforming. Moreover, recently [11] the researchers have tried to use the zeolite to prepare catalysts for methane reforming and have found that zeolite can be good support for the preparation of stable and active catalysts for this reaction if it is dealuminated and modified with transitions metals. Thus, we have prepared our

* Corresponding author at: Lodz University of Technology, Institute of General and Ecological Chemistry, Zeromskiego 116, 90 924 Lodz, Poland.
Tel.: +48 42 631 31 34.
** Corresponding author at: CNRS-UMR 7197, Laboratoire de Réactivité de Surface, Case 178, Site d'Ivry-Le Raphaël, 3 rue Galilée, 94200 Ivry sur Seine, France.
Tel.: +33 1 44 27 21 13.
E-mail addresses: karolinachalupka@op.pl (K.A. Chalupka), stanislaw.dzwigaj@upmc.fr (S. Dzwigaj).

0926-3373/$ – see front matter © 2013 Elsevier B.V. All rights reserved.
http://dx.doi.org/10.1016/j.apcatb.2013.05.007

Ni-loaded zeolite catalysts in particular conditions (by two-step postsynthesis method which consist firstly, dealumination of BEA zeolite and secondly, incorporation of Ni into framework of resulted SiBEA) and tested in severe reaction conditions to better understand their stability at high temperatures and resistance towards carbon deposition.

In this work, the influence of the preparation procedure and Ni content on the catalytic activity of Ni-containing BEA zeolites in POM reaction was investigated. The zeolite catalysts were characterized by DR UV–vis, TPR-H_2, TPO, TEM, XRD, TG-DTA-MS and TPD-NH_3.

2. Experimental

2.1. Samples preparation

Nickel-containing BEA zeolites were prepared by a conventional wet impregnation method and a two–steps postsynthesis procedure, which make it possible to control the introduction of Ni ions in the zeolite framework [12]. A tetraethylammonium BEA (TEABEA) zeolite provided by RIPP (China) was separated into two fractions. The first one was calcined (air, 15 h, 550 °C) in order to obtain an organic - free AlBEA zeolite (Si/Al = 11). The Ni_xAlBEA zeolites were prepared by impregnation of AlBEA with an aqueous solution of $Ni(NO_3)_2{\cdot}6H_2O$ (pH 2.6) under aerobic conditions [12–14]. Then the suspensions were stirred for 2 h at 80 °C until evaporation of water. The resulting solids were dried in air at 80 °C for 24 h and labeled Ni_xAlBEA. Then these solids were calcined in static air at 500 °C for 3 h and labeled C-Ni_xAlBEA. After treatment with H_2 flow at 550 °C for 1 h the samples were labeled Red-C-Ni_xAlBEA.

The second fraction of TEABEA was treated in a 13 mol dm^{-3} HNO_3 aqueous solution (4 h, 80 °C) to obtain a dealuminated and organic – free SiBEA support (Si/Al = 1300) with vacant T sites (T = Al). SiBEA was then recovered by centrifugation, washed with distilled water and dried at 80 °C. To incorporate nickel ions in vacant T sites, 2 g of SiBEA were stirred under aerobic conditions for 24 h at 25 °C in 200 cm^3 of $Ni(NO_3)_2{\cdot}6H_2O$ aqueous solution (pH 2.4–2.6) with different concentrations to obtain the zeolites with various Ni content [12–14]. Then the suspensions were stirred for 2 h at 80 °C until water was evaporated and the resulting solids were dried in air at 80 °C for 24 h and labelled Ni_xSiBEA. Then Ni_xSiBEA were calcined in static air at 500 °C for 3 h and the obtained solids were labeled C-Ni_xSiBEA. After treatment with H_2 flow at 550 °C for 1 h, the samples were labeled Red-C-Ni_xSiBEA.

2.2. Method of characterization

2.2.1. DR UV–vis

DR UV–vis spectra were recorded under ambient atmosphere on a Cary 5000 Varian spectrometer equipped with a double integrator with polytetrafluoroethylene as reference.

2.2.2. TPR-H_2

The TPR-H_2 measurements were carried out in an automatic TPR system (AMI-1) in the temperature range 25–900 °C, using H_2 stream (5% H_2–95% Ar). H_2 consumption was monitored by a thermal conductivity detector (TCD). The measurements were carried out in the system TPO-TPR-TPO-TPR (temperature programmed oxidation (in O_2 flow at 500 °C)-temperature programmed reduction (in 5% H_2–95% Ar flow 40 cm^3 min^{-1})).

2.2.3. TPD-NH_3

The TPD-NH_3 measurements were carried out in a quartz reactor using gaseous ammonium. The gaseous NH_3 was adsorbed in the zeolite catalysts at 100 °C for 10 min after drying in flowing He at 500 °C for 30 min, or after reduction of samples at 550 °C for 60 min in flowing H_2. All samples were calcined at 500 °C for 3 h in static air before each TPD-NH_3 experiment. The temperature programmed desorption of NH_3 was carried out in the temperature range 25–500 °C, after removing physisorbed ammonium from the catalyst.

2.2.4. XRD

Powder X-ray diffractograms were recorded on a PAN analytical X'Pert Pro MPD using Cu Kα radiation (λ = 154.05 pm) in the range of 2θ between 5 and 90°.

2.2.5. TEM EDX

The crystal morphology and the size of particles of Red-C-Ni_xAlBEA and Red-C-Ni_xSiBEA samples were identified by TEM (JEM-100 CX II ELECTRON MICROSCOPE, JEOL).

2.2.6. TOC analysis

Carbon deposit was defined by a total amount of carbon analyzed using an automatic analyzer of total carbon TOC 5000 with SSM 5000 (Shimadzu). The samples were combusted at 900 °C in oxygen flow (60 cm^3 min^{-1}). The product of combustion-CO_2 was analyzed using detector, working in the IR range.

2.2.7. TG-DTA-MS

Thermal analysis data (SETSYS 16/18, Setaram (France) and mass spectrometer ThermoStar, Balzers (Germany)) were used to define the formation of carbon deposit. The measurements were made from room temperature to 1000 °C in flowing air.

2.3. Catalytic tests

The catalytic activity test of partial oxidation of methane was carried out in a fixed bed reactor using a gas mixture of CH_4 and O_2 with a molar ratio of 2:1 (total gas flow: 75 cm^3 min^{-1}) and catalyst weight of 100 or 50 mg. The process was carried out under atmospheric pressure in the temperature range 300–900 °C. The reagents were analyzed by gas chromatograph. Before the catalytic test the catalysts were pretreated in static air at 500 °C for 3 h. The test of time of life of the catalysts was carried out for 12 h.

The reaction was analyzed by mass spectroscopy using the temperature programmed surface reaction (TPSR) method. The reaction were carried out in a quartz reactor using a gas mixture with the molar ratio of CH_4:O_2 = 2:1, in the temperature range 25–800 °C, using a linear heating rate 7 °C min^{-1}. The reactants and products were recorded by the MS detector.

3. Results and discussion

3.1. The nature of nickel species in C-Ni_xAlBEA and C-Ni_xSiBEA

DR UV–vis spectra of C-Ni_xAlBEA catalysts (C-Ni_1AlBEA, C-Ni_5AlBEA, C-Ni_{10}AlBEA) exhibit three main DR UV–vis bands at about 420, 535–590 and 720 nm (results not shown). The band at 420 and 535–590 nm can be attributed to the tetrahedral or distorted tetrahedral Ni(II) species and the band at 720 nm to the octahedral Ni(II) one, in line with the earlier reports [15–17]. However, C-Ni_xSiBEA catalysts exhibit only two main DR UV–vis bands at about 420 and 535–600 nm (results not shown), which can be attributed to the tetrahedral or distorted tetrahedral Ni(II) species [15–17].

3.2. The reducibility of C-Ni_xAlBEA and C-Ni_xSiBEA

Figs. 1 and 2 show TPR profiles for C-Ni_xAlBEA and C-Ni_xSiBEA catalysts after TPO-TPR-TPO-TPR cycles, respectively. It is well known that the strength of the interaction between the nickel

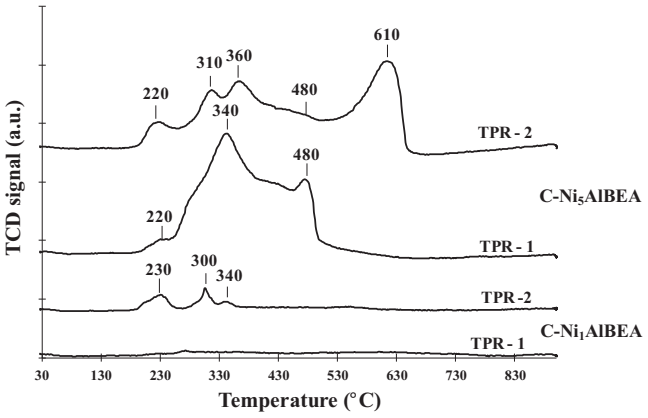

Fig. 1. TPR-H_2 profiles of C-Ni_1AlBEA and C-Ni_5AlBEA.

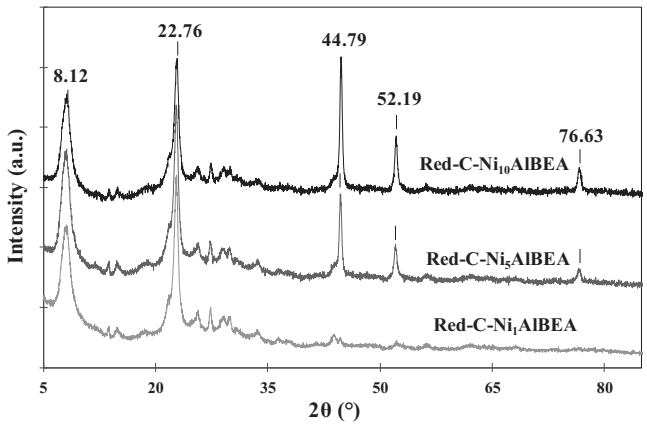

Fig. 3. XRD pattern recorded at room atmosphere of Red-C-Ni_1AlBEA, Red-C-Ni_5AlBEA and Red-C-Ni_{10}AlBEA after TPO-TPR-TPO-TPR measurements.

species and zeolite support can influence the course of the TPR process [18,19].

For C-Ni_1AlBEA with low Ni content, no reduction peak in the first TPR is observed. This can indicate a strong interaction of nickel with the AlBEA zeolite support and even the formation of nickel aluminosilicate, which is in line with earlier work by Pinheiro et al. [11]. In the second TPR, three small reduction peaks at 230, 300 and 340 °C appear. It is probable that the reoxidation of C-Ni_1AlBEA catalyst in air at 500 °C previously treated with H_2 at 900 °C leads to the weakening of the bond between the Ni species and zeolite support, and, in a consequence, its cracking. It could lead to the appearance of a small amount of octahedral Ni(II) species or NiO in extra-framework position of the BEA zeolite.

However, for higher Ni content (C-Ni_5AlBEA) three more intense reduction peaks appear with maximum at 220, 340 and 480 °C. They are related to the reduction of extraframework NiO and/or octahedral Ni(II) species (peaks at 220 and 340 °C) and pseudo-tetrahedral Ni(II) species (peak at 480 °C) located in the framework of zeolite, respectively [20,21]. A similar TPR pattern was obtained by Frontera et al. [20] on the Ni-BEA zeolite, where the reduction peak in temperature range 303–387 °C was assigned to the reduction of Ni(II) species, well dispersed in the zeolite structure [20]. In the second TPR of C-Ni_5AlBEA, five reduction peaks are observed with maximum at 220, 310, 340, 480 and 610 °C. The first four peaks can be related to the reduction of extraframework NiO and/or octahedral Ni(II) species (peaks at 220, 310 and 340 °C) and pseudo-tetrahedral Ni(II) species located in the framework of zeolite (peak at 480 °C). The last peak (at 610 °C) can be attributed to the reduction of nickel present as nickel aluminates, identified by TOF-SIMS investigation (results not shown).

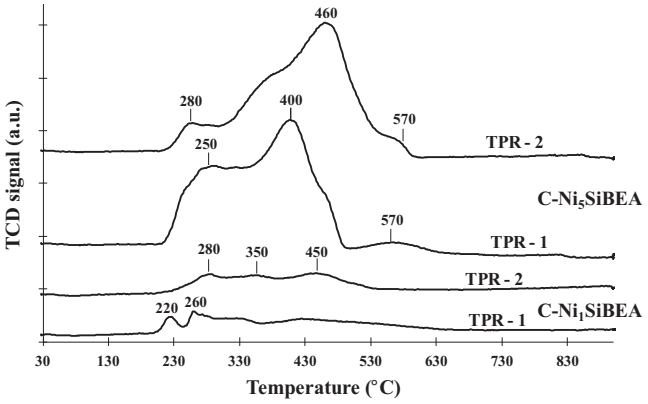

Fig. 2. TPR-H_2 profiles of C-Ni_1AlBEA and C-Ni_5AlBEA.

For C-Ni_1SiBEA, two reduction peaks with maximum at 220 and 260 °C are observed in the first TPR (Fig. 2), suggesting that at least two types of easily reducible nickel species are present in this sample, which is in line with the earlier report on NiSiBEA [18]. In the second TPR, one can observe three reduction peaks with maximum at 280, 350 and 450 °C. For C-Ni_5SiBEA with a much higher content of Ni, in the first and second TPR also three main reduction peaks appear with maximum at 250, 400 and 570 °C and 280, 460 and 570 °C, respectively. The main broad reduction peak at around 380–500 °C may be attributed to isolated pseudo-tetrahedral Ni(II) species strongly interacting with zeolite support, suggesting that this nickel species is incorporated in the framework of SiBEA zeolite, in agreement with earlier data on NiSiBEA [15] and Ni-containing A, X, Y and ZSM-5 zeolites [19]. The small peak at 570 °C may be assigned to the presence of the second kind of pseudo-tetrahedral Ni(II) related to the presence in the initial BEA zeolite of two kinds of framework tetrahedral Al(III) sites, as reported earlier [22]. Thus, dealumination of AlBEA zeolite followed by incorporation of nickel ion in vacant T-atom sites of SiBEA leads to two different kinds of tetrahedral Ni(II).

Moreover, the reduction peak at 250–280 °C can be attributed to the octahedral Ni(II) species or bulk NiO [23,24] present in a small amount in C-Ni_1SiBEA and in a much higher amount in C-Ni_5SiBEA.

The TPR results presented for C-Ni_1AlBEA and C-Ni_5AlBEA in Fig. 1 and for C-Ni_1SiBEA and C-Ni_5SiBEA in Fig. 2 suggest that nickel in the BEA zeolite structure can be present at least in three chemical environments which determine their reduction temperature. The much higher reduction temperature (about 610 °C) is related to the presence of nickel aluminates whose presence was confirmed by TOF-SIMS investigation (results not shown). The isolated pseudo-tetrahedral Ni(II) species strongly interacting with the zeolite support and present in the zeolite's framework are reduced also at a relatively high temperature (400–570 °C). The octahedral Ni(II) species and bulk NiO present in the extraframework position are reduced at a much lower temperature of 340 and 220–280 °C, respectively.

Our TPR results show that the reducibility of nickel strongly depends on its location in the zeolite structure, in line with the investigation by Garido Pedrosa et al. [21] and Velu et al. [25] on NiY.

3.3. XRD analysis of reduced C-Ni_xAlBEA and C-Ni_xSiBEA catalysts

X–ray powder diffractograms of Red–C-Ni_xAlBEA and Red-C-Ni_xSiBEA after the TPO–TPR cycles are presented in Figs. 3 and 4, respectively. For both Ni containing zeolites three main diffraction peaks at 2θ of 44.8, 52.2 and 76.6° appear. They correspond to

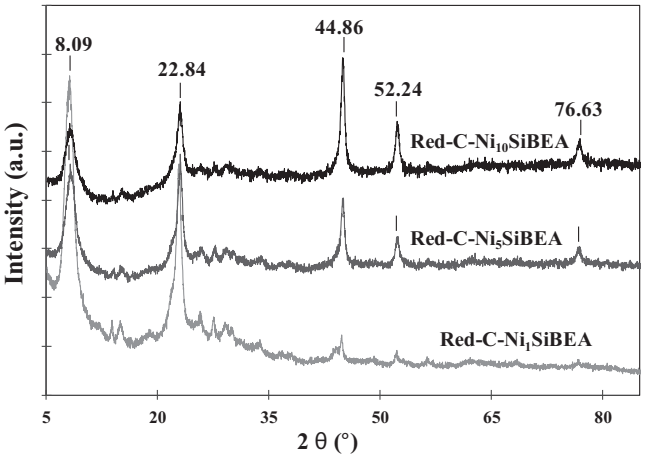

Fig. 4. XRD pattern recorded at room atmosphere of Red-C-Ni_1SiBEA, Red-C-Ni_5SiBEA and Red-C-Ni_{10}SiBEA after TPO-TPR-TPO-TPR measurements.

metallic Ni(0), which is in line with earlier literature data [26,27]. No diffraction peaks characteristic of the spinel phase, observed earlier for reduced Ni/Al_2O_3 catalyst at 2θ of 37, 45, 60 and 66° [26] can be seen. Moreover, two intense peaks at around 2θ of 8.10 and 22.80°, characteristic of the BEA zeolite present in all studied samples, indicate that the crystal structure of zeolite was not destroyed upon introduction of nickel in AlBEA and SiBEA zeolites and the following calcination and reduction of Ni_xAlBEA and Ni_xSiBEA. The change of the relative intensity of the diffraction peaks at 8.10 and 22.80° observed for Red-C-Ni_xAlBEA and Red-C-Ni_xSiBEA in Figs. 3 and 4 can be explained by the coexistence of several polytypes in BEA structure which transform one form into another as a result of the BEA zeolite treatments in BEA structure [28–33]. It seems that the incorporation of Ni ions in the framework of BEA zeolite additionally stabilizes the zeolite structure.

3.4. Acidity of C-Ni_xAlBEA and C-Ni_xSiBEA catalysts

The profiles of TPD - NH_3 for C-Ni_xAlBEA and C-Ni_xSiBEA and Red-C-Ni_xAlBEA and Red-C-Ni_xSiBEA are shown in Figs. 5 and 6, and Figs. 7 and 8, respectively. The desorption curves for C-Ni_1AlBEA and C-Ni_5AlBEA and C-Ni_1SiBEA and C-Ni_5SiBEA in Figs. 6 and 7 show only one desorption peak with its maximum at 180–220 °C, related to weak acidic sites, in line with earlier work [34]. For C-Ni_{10}AlBEA with a much higher content of Ni, a desorption peak at 590 °C is observed, which corresponds to the strong acidic sites and is in agreement with earlier work [34]. These strong acidic sites are probably connected with the presence of nickel oxide and/or octahedral Ni(II) species in the extraframework position. Our TPD - NH_3 results are in good agreement with the work by Pinheiro et al. [11], who observed the peaks in the temperature range 117–350 °C, assigned to weak and medium Lewis acid sites, and the peak in the temperature range 350–577 °C, assigned to Brønsted acidic sites.

For Red-C-Ni_xAlBEA and Red-C-Ni_xSiBEA samples obtained after reduction in flowing H_2 at 550 °C for 1 h, the desorption curves can be deconvoluted and fitted by two and three peaks respectively with maximum temperatures at 210–220 and 500–515 °C for Red-C-Ni_xAlBEA and at 150–170, 340–410 and 510–520 °C for Red-C-Ni_xSiBEA. These peaks correspond to desorption of ammonia from weak, medium and strong acidic sites, respectively [34].

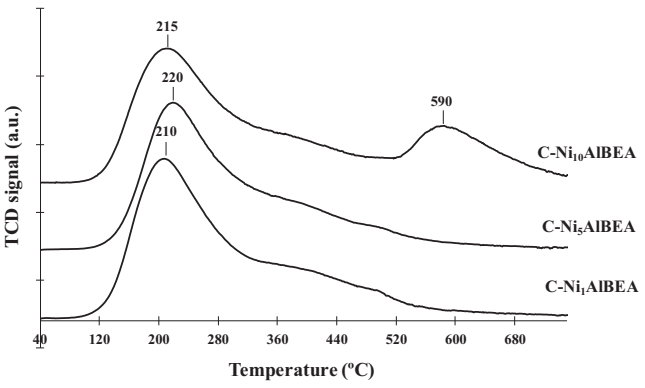

Fig. 5. TPD-NH_3 profiles of C-Ni_1AlBEA and C-Ni_5AlBEA.

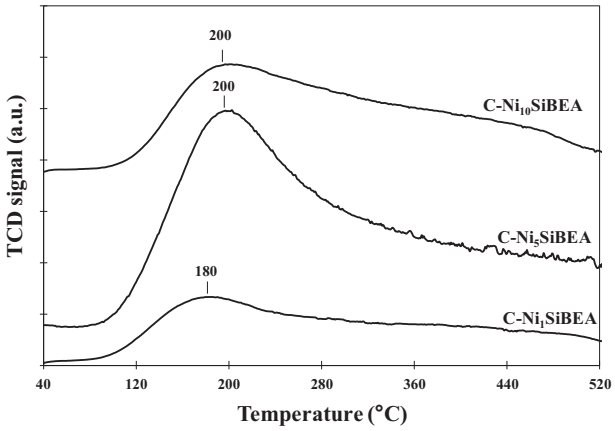

Fig. 6. TPD-NH_3 profiles of C-Ni_1SiBEA and C-Ni_5SiBEA.

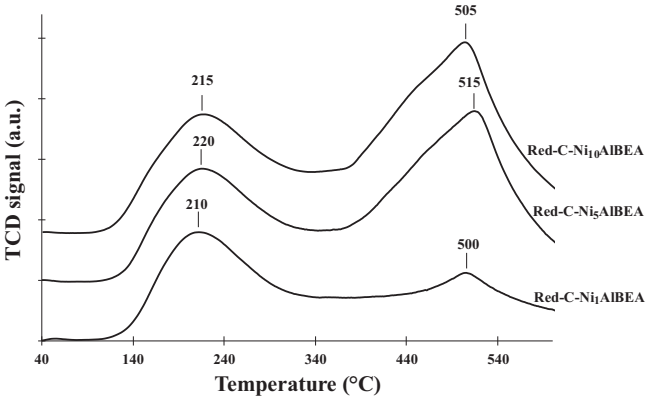

Fig. 7. TPD-NH_3 profiles of Red-C-Ni_1AlBEA, Red-C-Ni_5AlBEA and Red-C-Ni_{10}AlBEA.

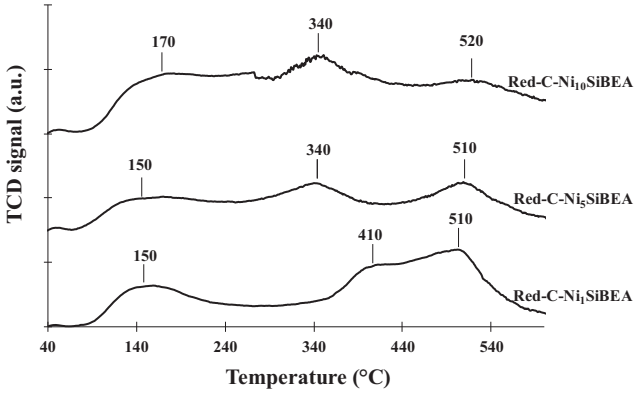

Fig. 8. TPD-NH_3 profiles of Red-C-Ni_1SiBEA, Red-C-Ni_5SiBEA and Red-C-Ni_{10}SiBEA.

Table 1
Concentration of acidic sites measured by using TPD–NH_3 method.

Sample	Total amount of NH_3 adsorbed after calcination at 500 °C for 3 h ($\mu mol\ g^{-1}$)	Total amount of NH_3 adsorbed after reduction in H_2 flow at 550 °C for 1 h ($\mu mol\ g^{-1}$)
AlBEA	2410	–
SiBEA	320	–
Ni_1AlBEA	2540	21.37
Ni_5AlBEA	2530	29.38
Ni_{10}AlBEA	2990	31.85
Ni_1SiBEA	770	7.58
Ni_5SiBEA	2310	4.32
Ni_{10}SiBEA	1340	5.09

The amount of ammonia desorbed and the desorption temperature were regarded as a measure of total acidity and acid strength of catalysts. The introduction of Ni ions into SiBEA and AlBEA zeolites causes an increase in the total amount of acidic sites (Table 1). By contrast, the reduction of C-Ni_xAlBEA and C-Ni_xSiBEA with hydrogen involves significant decreases of these sites. Indeed, the amount of ammonia adsorbed on C-Ni_xAlBEA and C-Ni_xSiBEA decreases significantly (Table 1) after reduction in flowing H_2 from 2530–2999 $\mu mol\ g^{-1}$ for C-Ni_xAlBEA to 21.37–31.85 $\mu mol\ g^{-1}$ for Red-C-Ni_xAlBEA and from 770–2310 $\mu mol\ g^{-1}$ for C-Ni_xSiBEA to 4.32–7.58 $\mu mol\ g^{-1}$ for Red-C-Ni_xSiBEA. These findings can indicate the creation of new nickel species during reduction processes and the formation of metallic Ni.

3.5. Nickel particles sizes in reduced C- Ni_xAlBEA and C-Ni_xSiBEA catalysts

The morphology of reduced C-Ni_xAlBEA and C-Ni_xSiBEA samples was investigated by using TEM (Figs. 9 and 10, Table 2). In Fig. 9, TEM images of Red-C-Ni_1AlBEA (a), Red-C-Ni_1SiBEA (b) and Red-C-Ni_5SiBEA (c) are presented. They show the typical shape and channels of synthesized BEA zeolite nanocrystals and small nickel particles [35,36]. As shown in Table 2, the average particle size of Ni is 5 nm for Red-C-Ni_5SiBEA and 9 nm for Red-C-Ni_{10}SiBEA. For Red-C-Ni_xAlBEA, the average particle size is much higher than for Red-C-Ni_xSiBEA. It is 12 nm for Red-C-Ni_1AlBEA and 26 nm for Red-C-Ni_{10}AlBEA (Table 2).

The TEM studies of the samples after POM reaction are presented in Fig. 10 and Table 2. They show that the morphology of Red-C-Ni_xAlBEA and C-Ni_xSiBEA does not change after reaction. The characteristic structure of zeolite is preserved (Fig. 10). However, the particle size of Ni is even twice as high as before the reaction. For Red-C-Ni_xSiBEA, it changes from 5–9 nm to 9–17 nm and for Red-C-Ni_xAlBEA from 12–26 to 22–33 nm (Table 2). This is a result of agglomeration of Ni particles during the high temperature POM reaction and the most probable reason for deactivation of C-Ni_xAlBEA catalysts.

Table 2
Average particles size measured by TEM EDS.

Sample	Average particles size after reduction (nm)	Average particles size after POM reaction (nm)
Ni_1AlBEA	11.80	–
Ni_1SiBEA	5.74	8.65
Ni_5AlBEA	–	22.71
Ni_5SiBEA	4.86	12.43
Ni_{10}AlBEA	25.58	32.50
Ni_{10}SiBEA	8.86	16.65

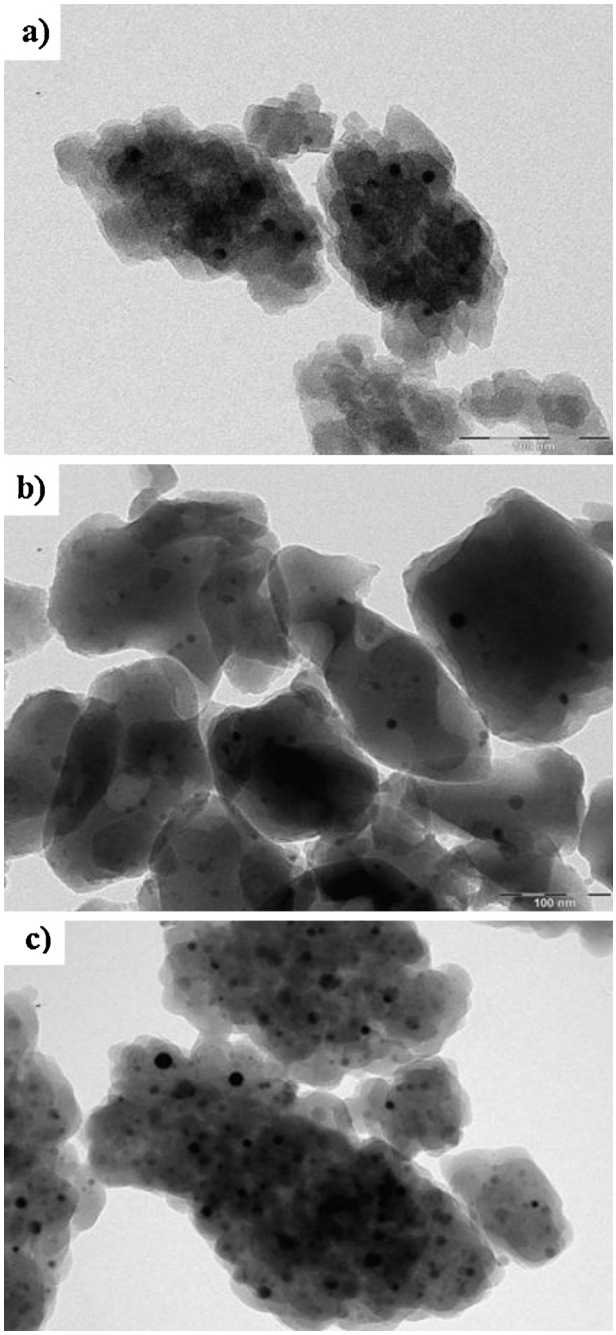

Fig. 9. TEM of Red-C-Ni_1AlBEA (a), Red-C-Ni_1SiBEA (b) and Red-C-Ni_5SiBEA (c).

3.6. The catalytic activity and thermal stability of C-Ni_xAlBEA and C-Ni_xSiBEA catalysts

The activities of C-Ni_xAlBEA and C-Ni_xSiBEA zeolites in partial oxidation of methane (POM) were investigated in detail. The results of POM are collected in Table 3 (for 50 and 100 mg of sample weight) and presented in Figs. 11–14 as CH_4 conversion and selectivity to CO versus temperature (for the mass of sample of 50 and 100 mg) and in Figs. 15 and 16 as CH_4 conversion and selectivity to CO versus time (for 50 mg of sample weight) for C-Ni_xSiBEA (Figs. 13–15) and C-Ni_xAlBEA (Figs. 11, 12, 16) catalysts, respectively. The results indicate that all C-Ni_xSiBEA are active in POM reaction independently of the sample weight (Figs. 13, 14 and Table 3) and allow a very high methane conversion (Figs. 13, 14 and 15a) and selectivity to

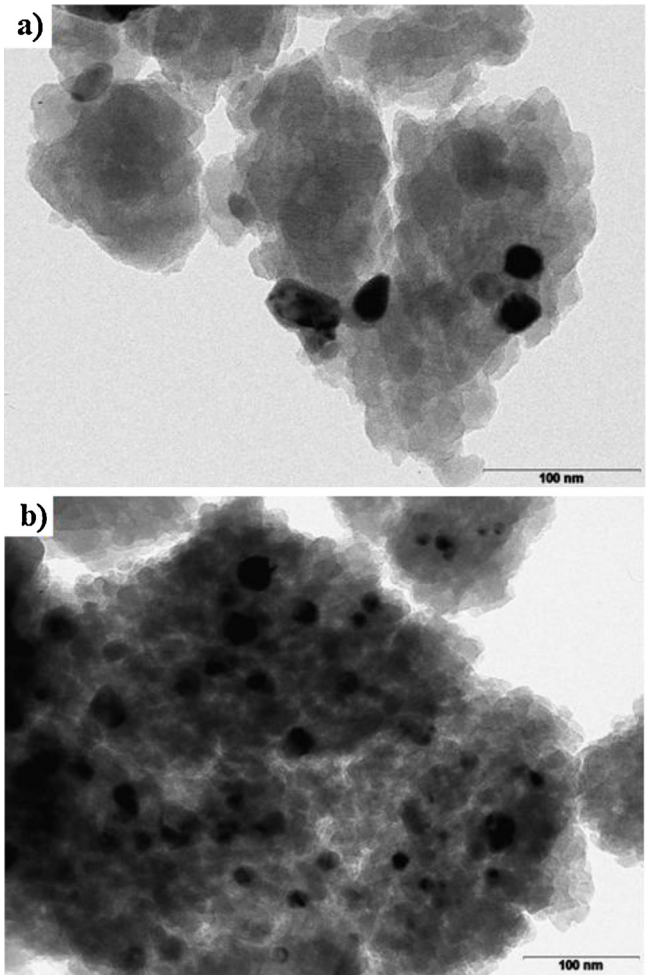

Fig. 10. TEM of C-Ni_5AlBEA (a) and C-Ni_5SiBEA (b) after POM reaction.

Table 3
Temperature at which both CH_4 conversion and the selectivity to CO is 100%.

Sample	Temperature for S_{CO} = 100% and K_{CH_4} = 100% (°C)		Amount of carbon deposition measured by TOC analyzer (%)
	m = 50 mg	m = 100 mg	
C-Ni_1AlBEA	–	875 (S_{CO} < 100%)	0.0
C-Ni_5AlBEA	700[a]	750	0.0
C-Ni_{10}AlBEA	800[b]	725	0.0
C-Ni_1SiBEA	875[c]	875[d]	0.0
C-Ni_5SiBEA	800	750	0.0
C-Ni_{10}SiBEA	750	750	0.0

[a] Catalytic activity decreases after a few hours of the reaction.
[b] Catalytic activity decreases after a few hours of the reaction.
[c] Conversion of methane K_{CH_4} < 100%.
[d] Selectivity to CO is 100% after 1 h of the reaction.

CO (Figs. 13, 14 and 15b) close to 100%. Only for C-Ni_1SiBEA catalyst, a decrease in the sample mass from 100 to 50 mg lowers CH_4 conversion to about 20–25%. However, 100% selectivity to CO is maintained for all the catalysts under study.

C-Ni_xAlBEA catalyst containing only 1 wt.% of Ni shows poor activity in POM reaction, as shown in Table 3 and Fig. 12. The selectivity to CO on this sample is lower than 100%. The reason for such behaviour is very low reducibility of nickel species, proved by an absence of TPR peaks in C-Ni_1AlBEA (Fig. 1, TPR-1). The samples with a higher content of Ni (5 and 10 wt.%) are active in POM reaction, showing both very high CH_4 conversion and CO selectivity (100%), (Table 3, Figs. 11 and 12). However, the use of lower sample weight in the catalytic activity tests leads to the decrease in CH_4 conversion (Figs. 11 and 16a), but the selectivity to CO is still very high (100%) (Fig. 16b).

The most active catalysts are C-Ni_xSiBEA with 5 and 10 wt.% of Ni content. The temperature at which they exhibit high selectivity to CO and CH_4 conversion (100%) is about 125 °C lower than for C-Ni_1SiBEA. Moreover, C-Ni_xSiBEA catalysts are more stable than

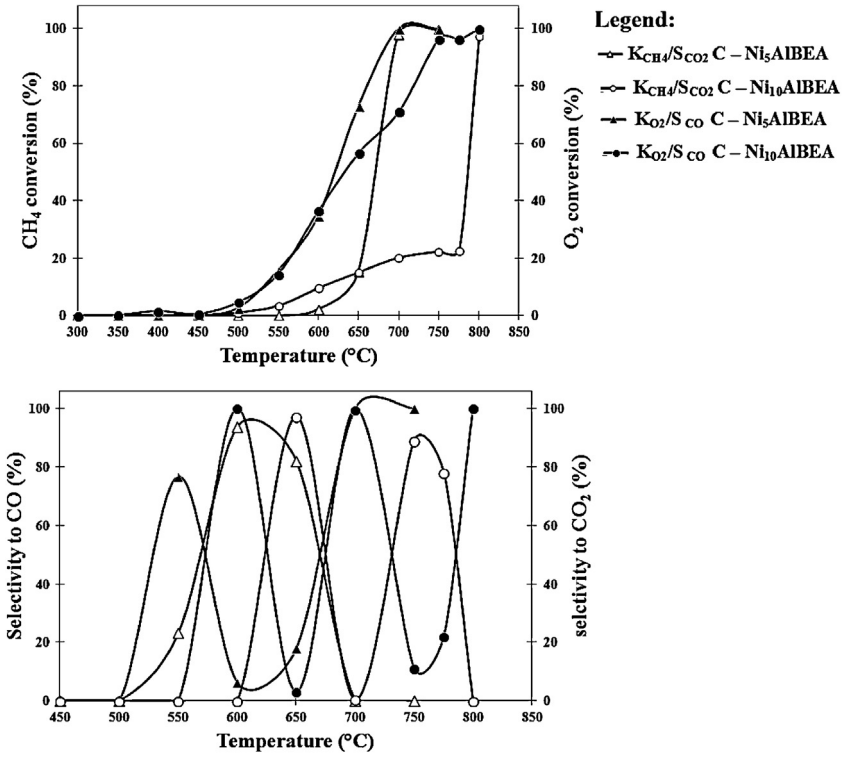

Fig. 11. Catalytic performance of C-Ni_5AlBEA and C-Ni_{10}AlBEA (samples weight of 50 mg).

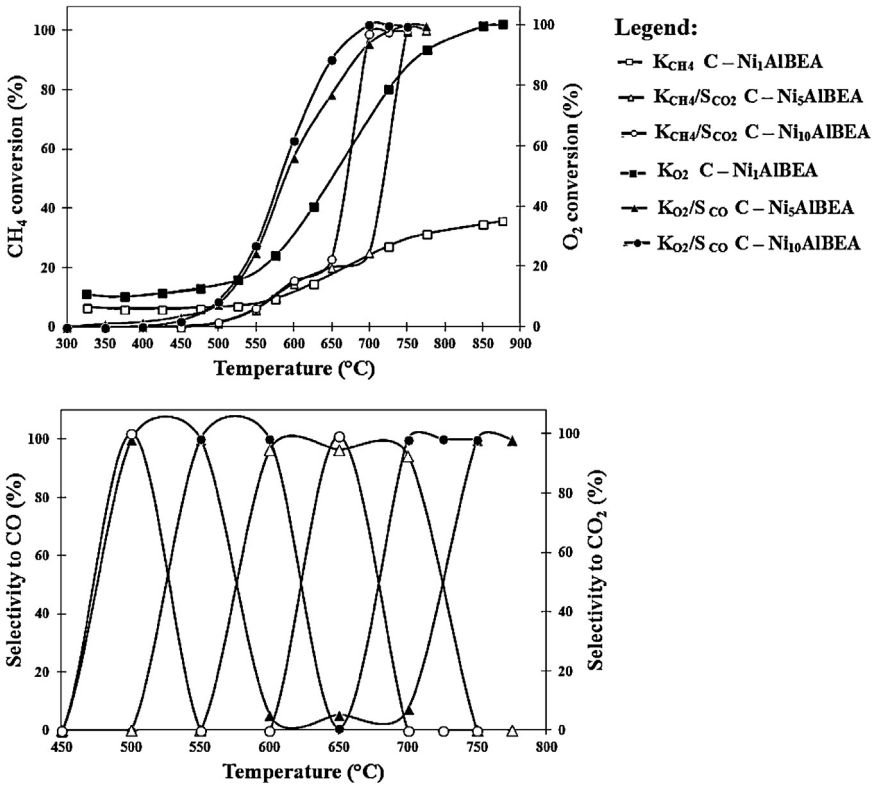

Fig. 12. Catalytic performance for C-Ni_1AlBEA, C-Ni_5AlBEA and C-Ni_{10}AlBEA (samples weight of 100 mg).

C-Ni_xAlBEA and do not deactivate even after 14 h of work. It shows that dealumination in the first step of preparation and then incorporation of nickel ions into the framework of SiBEA zeolite support improve the activity of catalysts. For C-Ni_xSiBEA zeolites, nickel is present in framework as tetrahedral Ni(II) species, as evidenced by DR UV–vis (the result not shown), strongly bonded to the zeolite support. Such a localization of Ni(II) ions prevents an agglomeration of nickel particles and stabilizes C-Ni_xSiBEA catalysts [37].

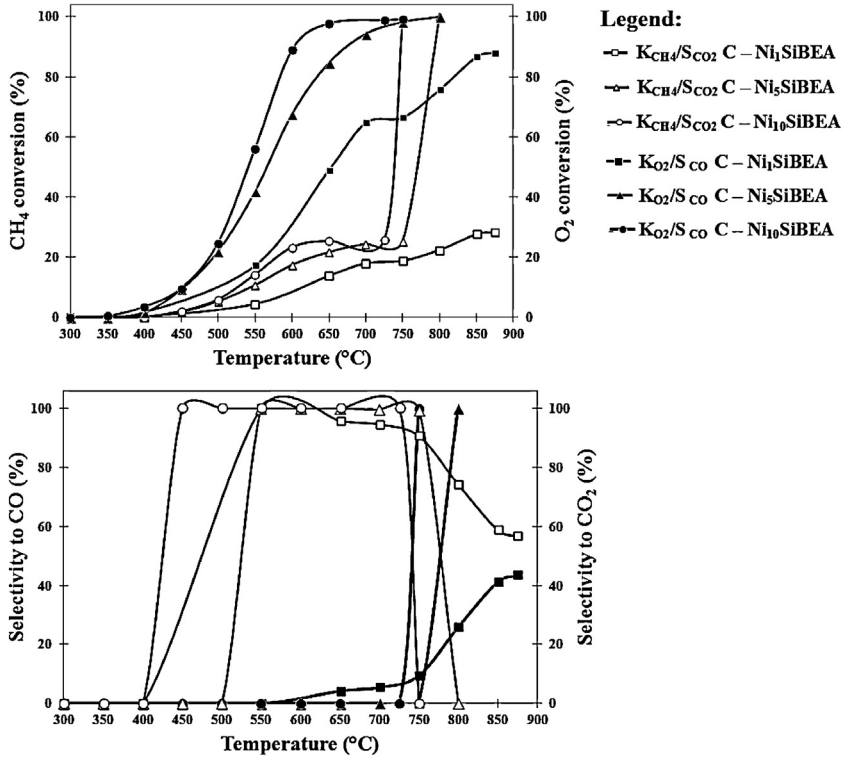

Fig. 13. Catalytic performance of C-Ni_1SiBEA, C-Ni_5SiBEA and C-Ni_{10}SiBEA (samples weight of 50 mg).

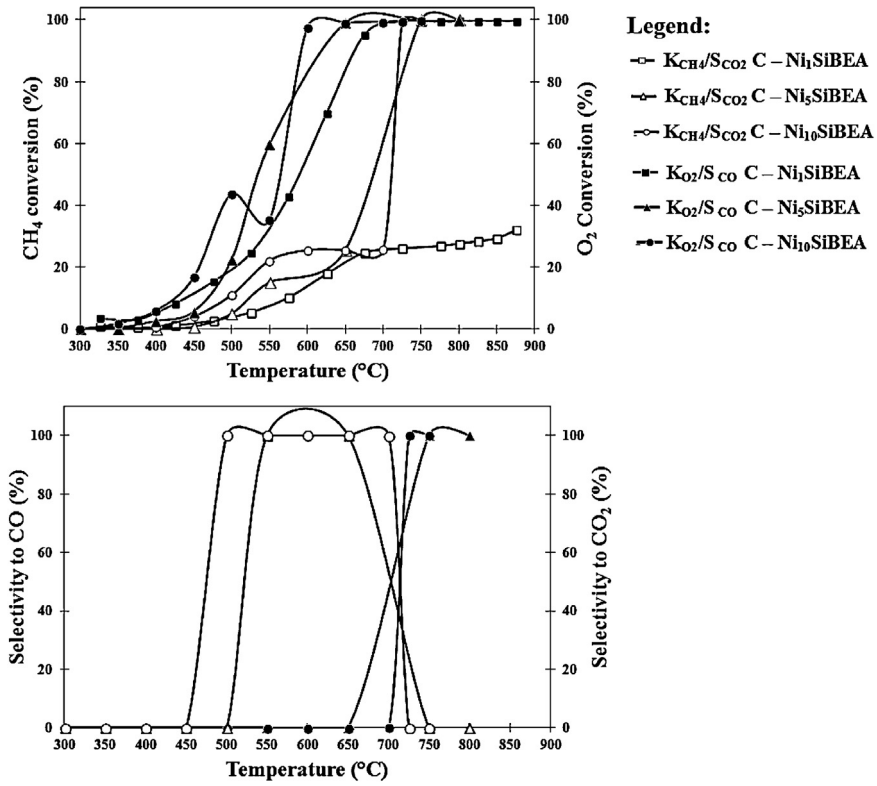

Fig. 14. Catalytic performance for C-Ni_1SiBEA, C-Ni_5SiBEA and C-Ni_{10}SiBEA (samples weight of 100 mg).

Thus, a much better dispersion of nickel particles takes place in Red – C-Ni_xSiBEA than in Red-C-Ni_xAlBEA, which is shown in the TEM studies. It is important to underline that for all C-Ni_xAlBEA and C-Ni_xSiBEA catalysts carbon deposition is not observed (Table 3). This suggests that deactivation of C-Ni_xAlBEA catalysts may be connected with easier sintering of nickel species in these catalysts than in C-Ni_xSiBEA (Table 2).

The profiles of TG-DTA-MS analysis of C-Ni_{10}SiBEA and C-Ni_{10}AlBEA after POM reaction are presented in Fig. 17. They show higher weight loss for C-Ni_{10}AlBEA (7.9%) than for C-Ni_{10}SiBEA (0.8%). However, these weight losses can be related to the removal of H_2O, CO and O_2, observed on MS profiles. For Ni_{10}SiBEA catalyst, the amount of released CO_2 remains constant in all the

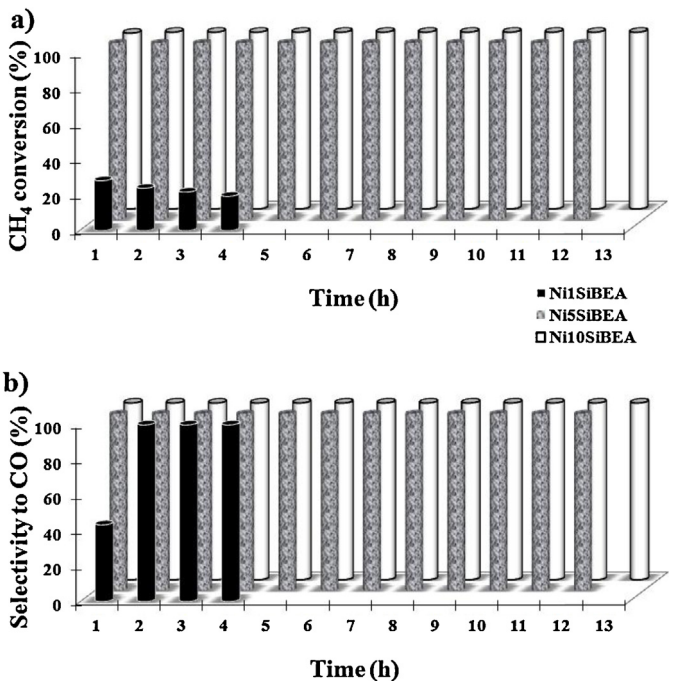

Fig. 15. CH_4 conversion (a) and selectivity to CO (b) plotted as a function of time for C-Ni_1SiBEA, C-Ni_5SiBEA and C-Ni_{10}SiBEA (samples weight of 50 mg).

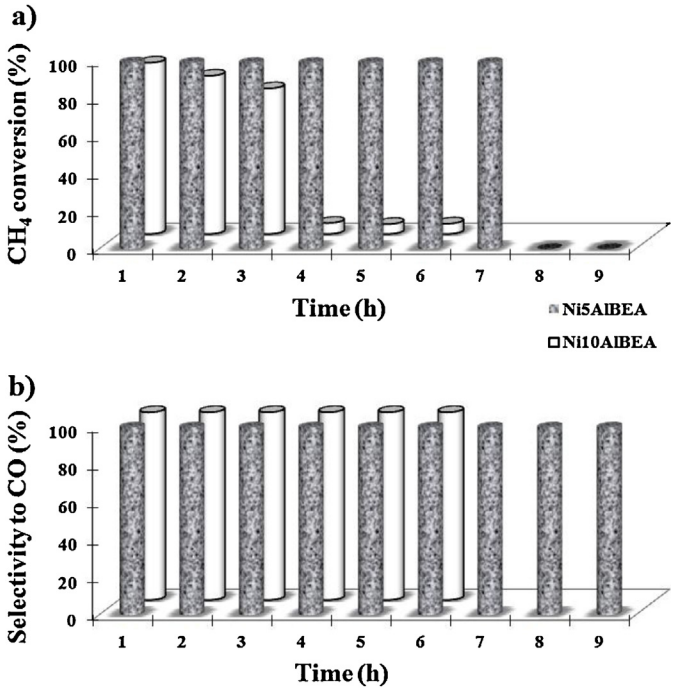

Fig. 16. CH_4 conversion (a) and selectivity to CO (b) plotted as a function of time for C-Ni_5AlBEA and C-Ni_{10}AlBEA (samples weight of 50 mg).

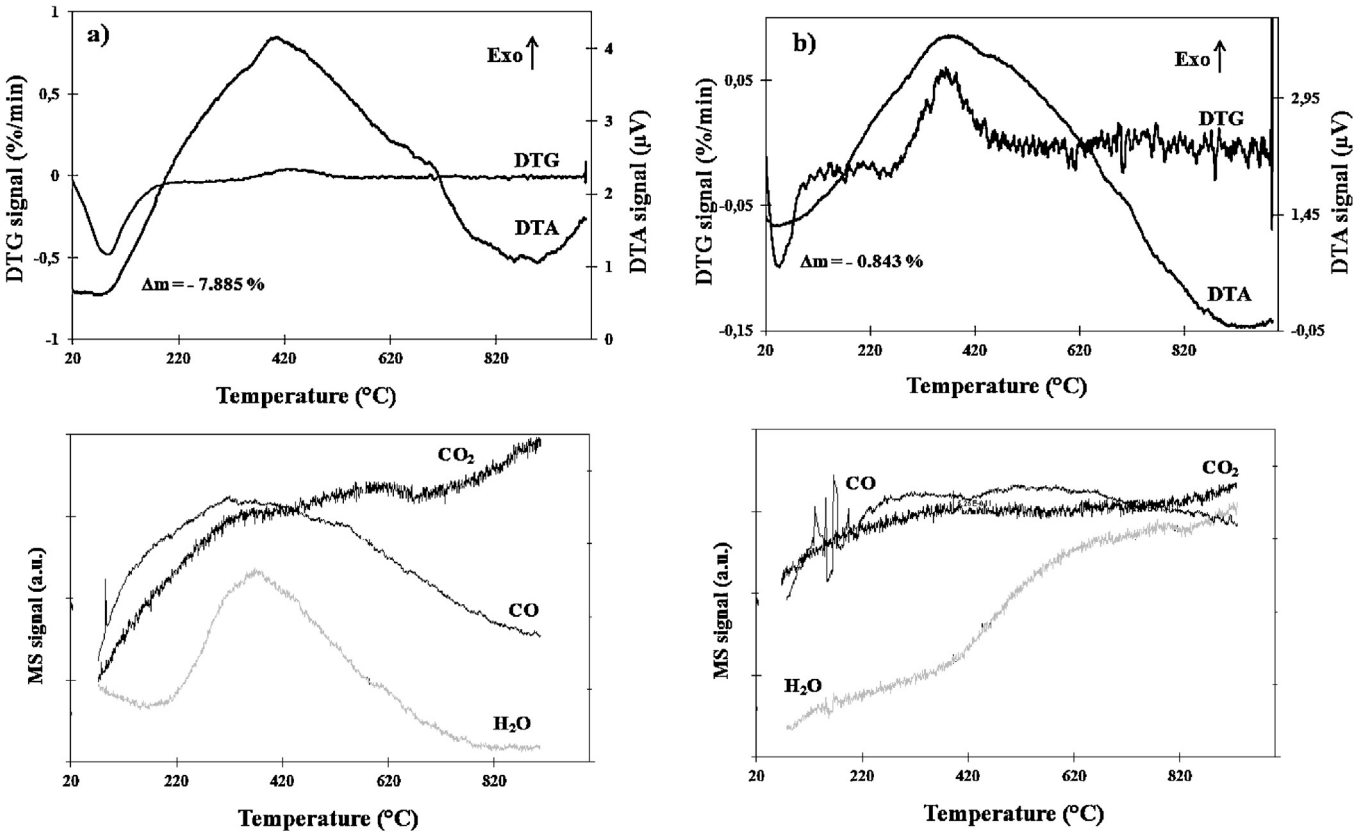

Fig. 17. Thermal analysis of Ni_{10}AlBEA (a) and Ni_{10}SiBEA (b) catalysts after POM reaction.

studied temperature range, which indicates the lack of carbon deposit (Fig. 17b). In the case of C-Ni_{10}AlBEA catalyst, the amount of involved CO_2 slightly increases, which is probably connected with the oxidation of removed CO (Fig. 17a).

The reaction was analyzed with the use of the MS spectrometer, which allows detecting reagents and products of POM reaction. In Figs. 18 and 19, MS profiles for C-Ni_5AlBEA and C-Ni_5SiBEA catalysts are presented. In literature, the POM mechanism was widely studied for different Ni supported catalysts. The researchers divided it into two categories: the first one is the indirect oxidation mechanism involving methane total combustion and steam and dry reforming reactions, which is called the "combustion and reforming reaction mechanism" (CRR), and the second one is the direct oxidation mechanism (DPO), which assumes that surface carbon and oxygen species react to form primary products [37,6].

MS profiles for C-Ni_5AlBEA (Fig. 18) and C-Ni_5SiBEA (Fig. 19) catalysts are similar and show that O_2 begins to be consumed at around 420–425 °C and at the same temperature CH_4 consumption started. The conversion of CH_4 and O_2 increases with the rise in temperature. One can observe the total consumption of O_2 at 725 °C for C-Ni_5AlBEA and at 600 °C for C-Ni_5SiBEA sample. It indicates that the consumption of O_2 occurs much faster on C-Ni_5SiBEA. The formation of CO_2 and H_2O, as the only products, occurs in the temperature range 425–770 °C for C-Ni_5AlBEA and 420–720 °C for C-Ni_5SiBEA, which means that in these temperature ranges methane is completely oxidized (reaction 1). From the temperature of 770 °C for C-Ni_5AlBEA and 725 °C for C-Ni_5SiBEA catalysts, the full conversion of CH_4 is observed and CO and H_2 are formed as the only products (reaction 4). The formation of CO and H_2 can result not only from the reaction of partial methane oxidation, but

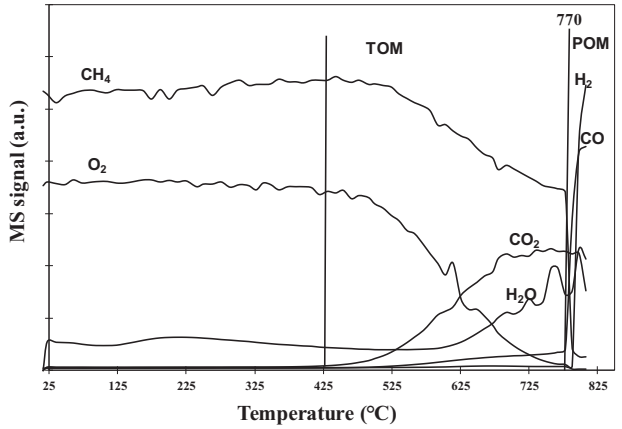

Fig. 18. POM TPSR profiles of C-Ni_5AlBEA.

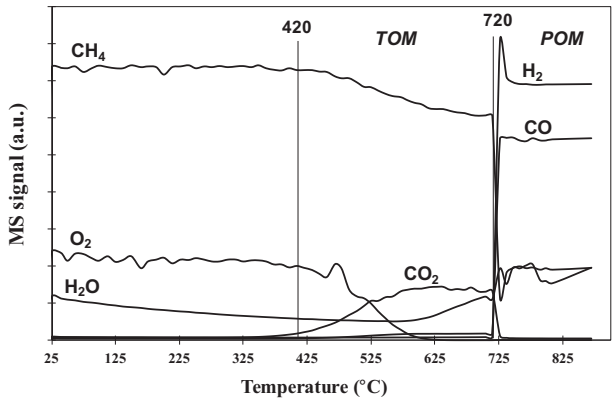

Fig. 19. POM TPSR profiles of C-Ni_5SiBEA.

also from dry and steam reforming of CH_4 (reactions (2) and (3)). For Ni_xSiBEA catalysts, it was observed that in the temperature range from 500 to 700 °C the conversion of O_2 is close to 100% and that of CH_4 is close to 25%, and the only product is CO_2 (Figs. 13 and 14). In the temperature range between 700 and 800 °C the conversion of both O_2 and CH_4 is complete and only CO is formed (Figs. 13 and 14). For Ni_xAlBEA catalysts in the temperature range from 500 to 550 °C CO is formed, which can result from very small O_2 consumption, insufficient for the total oxidation of methane (conversion of O_2 is only 15% for Ni_5AlBEA and 30% for Ni_{10}AlBEA). In the higher temperature range (550 – 700 °C), the formation of CO_2 predominates (selectivity to CO_2 is between 80 and 100%), whereas only a small amount of CO is formed (the conversion of O_2 at this temperature is between 60 and 90% and the conversion of CH_4 is near 25%). In the temperature range 700–800 °C the only product is CO (Figs. 11 and 12).

The POM reaction can proceed through the following indirect reactions:

a) total oxidation of methane (TOM):

$$CH_4 + 2O_2 \rightarrow CO_2 + 2H_2O \quad (1)$$

b) dry and steam reforming of methane:

$$CH_4 + CO_2 \rightarrow 2CO + 2H_2 \quad (2)$$

$$CH_4 + H_2O \rightarrow CO + 3H_2 \quad (3)$$

c) partial oxidation of methane (POM):

$$CH_4 + \frac{1}{2}O_2 \rightarrow CO + 2H_2 \quad (4)$$

This may indicate that the POM reaction on C-Ni_5AlBEA and C-Ni_5SiBEA zeolite catalysts proceeds according to the CRR mechanism. Similar results for Ni/α–Al_2O_3 catalysts were obtained by Jin and co-workers [38]. They postulated that in the first step CH_4 interacts with NiO species, which leads to the total oxidation of CH_4 and simultaneous reduction of NiO to Ni^0 (Eq. (5)) and in the second step CH_4 dissociates over Ni^0 particles, and Ni···C species are created and H_2 is formed (Eq. (6)). The Ni···C species can further react with the $Ni^{\gamma+}\cdots O^{\gamma-}$ species derived from O_2 activation, forming CO as a primary product (Eq. (7)) [38].

$$3NiO + CH_4 + \frac{1}{2}O_2 \rightarrow 3Ni^0 + CO_2 + 2H_2O \quad (5)$$

$$Ni^0 + CH_4 \rightarrow Ni\cdots C + 2H_2 \quad (6)$$

$$Ni\cdots C + Ni\cdots O \rightarrow CO + Ni^0 \quad (7)$$

4. Conclusion

Two different catalytic systems based on BEA zeolites were obtained by two preparation methods: C-Ni_xAlBEA by a conventional wet impregnation method and C-Ni_xSiBEA by two-step postsynthesis method. These catalytic systems show different physicochemical properties related to Ni species being in a weak or strong interaction with the zeolite support.

C-Ni_xSiBEA shows a very good catalytic activity in POM and high stability. The 100% of methane conversion and 100% selectivity to CO are reached for C-Ni_5SiBEA and C-Ni_{10}SiBEA catalysts at 750 °C. C-Ni_xSiBEA catalysts are significantly resistant to deactivation.

For both series of C-Ni_xSiBEA and C-Ni_xAlBEA catalysts under study, one cannot observe the formation of carbon deposit, in contrast to the catalysts used so far and described in literature.

C-Ni_xSiBEA catalysts are characterized by higher thermal stability than C-Ni_xAlBEA, which indicates that dealumination decreasing the acidity of samples improves thereby their catalytic activity.

Acknowledgements

This work is financed by National Science Center (Poland) (Grant no. 7621/B/H03/2011/40)

References

[1] J.H. Jun, T.H. Lim, S.W. Nam, S.A. Hong, K.J. Yoon, Applied Catalysis A 312 (2006) 27–34.
[2] F. Pompeo, N.N. Nichio, O.A. Ferreti, D. Resasco, International Journal of Hydrogen Energy 30 (2006) 1399–1405.
[3] Q.G. Yan, T.H. Wu, W.Z. Weng, H. Toghiani, R.K. Toghiani, H.L. Wan, C.U. Pittman Jr., Journal of Catalysis 226 (2004) 247–259.
[4] S. Freni, G. Calogero, S. Cavallaro, Journal of Power Sources 87 (2000) 28–38.
[5] Y. Zhang, Z. Li, X. Wen, Y. Liu, Chemical Engineering Journal 121 (2006) 115–123.
[6] A.P.E. York, T. Xiao, M.L.H. Green, Topics in Catalysis 22 (3–4) (2003) 345–358.
[7] J. Weitkamp, Solid State Ionics 131 (2000) 175–188.
[8] S. van Donk, A.H. Janssen, J.H. Bitter, K.P. de Jong, Catalysis Reviews 45 (2003) 297–319.
[9] B. Wichtelová, Z. Sobalık, J. Dědček, Applied Catalysis B 41 (2003) 97–114.
[10] A. Corma, Journal of Catalysis 216 (2003) 298–312.
[11] A.N. Pinheiro, A. Valentini, J.M. Sasaki, A.C. Oliveira, Applied Catalysis A 355 (2009) 156–168.
[12] S. Dzwigaj, M. Che, Journal of Physical Chemistry B 110 (2006) 12490–12493.
[13] J. Janas, T. Shishido, M. Che, S. Dzwigaj, Applied Catalysis B 89 (2009) 196–203.
[14] J. Janas, T. Machej, J. Gurgul, R.P. Socha, M. Che, S. Dzwigaj, Applied Catalysis B 75 (2007) 239–248.
[15] S. Bendezu, et al., Applied Catalysis A 197 (2000) 47–60.
[16] L. Chen, et al., Applied Catalysis A 209 (2001) 97–105.
[17] L. Espinosa-Alonso, Journal of Physical Chemistry C 112 (2008) 7201–7209.
[18] A. Penkova, S. Dzwigaj, R. Kefirov, K. Hadjivanov, M. Che, Journal of Physical Chemistry C 111 (2007) 8623–8631.
[19] A. Luengnaruemitchai, A. Kaengsilalai, Chemical Engineering Journal 144 (2008) 96–102.
[20] P. Frontera, A. Aloise, A. Macario, P.L. Antonucci, F. Crea, G. Giordano, J.B. Nagy, Topics in Catalysis 53 (2010) 265–272.
[21] A.M. Garrido Pedrosa, M.J. Souza, D.M.A. Melo, A.S. Araujo, Materials Research Bulletin 41 (2006) 1105–1111.
[22] R. Hajjar, Y. Millot, P.P. Man, M. Che, S. Dzwigaj, Journal of Physical Chemistry C 112 (2008) 20167–20175.
[23] C.A. Tolman, W.M. Riggs, W.J. Linn, C.M. King, R.C. Wendt, Inorganic Chemistry 12 (1973) 2770–2778.
[24] K. Hadjiivanov, M. Mihaylov, D. Klissurski, P. Stefanov, N. Abadjieva, E. Vassileva, L. Mintchev, Journal of Catalysis 185 (1999) 314–323.
[25] S. Velu, Ch. Song, M.H. Engelhord, Y.H. Chin, Industrial & Engineering Chemistry Research 44 (2005) 5740–5749.
[26] G. Li, L. Hu, J.M. Hill, Applied Catalysis A 301 (2006) 16–24.
[27] P. Kim, Y. Kim, I.K. Song, J. Yi, Applied Catalysis A 272 (2004) 157–166.
[28] V. Valtchev, S. Mintova, Microporous and Mesoporous Materials 43 (2001) 41–49.
[29] A. Omegna, M. Vasic, J.A. van Bokhoven, G. Pirngruber, R. Prins, Physical Chemistry Chemical Physics 6 (2004) 447–452, Online available.
[30] S. Mintova, V. Valtcher, T. Onfroy, C. Marichal, H. Knözinger, T. Bein, Microporous and Mesoporous Materials 90 (2006) 237–245.
[31] J.B. Higgins, R.B. LaPierre, J.L. Schlenker, A.C. Rohrman, J.D. Wood, G.T. Kerr, W.J. Rohrbaugh, Zeolites 8 (1988) 446–452.
[32] J.M. Newsam, M.M.J. Treacy, W.T. Koetsier, C.B. Degruyter, Proceedings of the Royal Society of London A 420 (1988) 375–405.
[33] M.M.J. Treacy, J.M. Newsam, Nature 332 (1988) 249–251.
[34] A. Masalska, Catalysis Today 65 (2001) 271–277.
[35] F.S. Xiao, L. Wang, Ch. Yin, K. Lin, Y. Di, J. Li, R. Xu, D.S. Su, R. Schlogl, T. Yokoi, T. Tatsumi, Angewandte Chemie International Edition 45 (2006) 3090–3093.
[36] S. Lima, M.M. Antunes, A. Fernandes, M. Pillinger, M.F. Ribeiro, A.A. Valente, Applied Catalysis A 388 (2010) 141–148.
[37] Q. Zhu, X. Zhao, Y. Deng, Journal of Natural Gas Chemistry 13 (2004) 191–203.
[38] R. Jin, Y. Chen, W. Li, W. Cui, Y. Ji, Ch. Yu, Y. Jiang, Applied Catalysis A 201 (2000) 71–80.